Synthesis, characterization and anticancer studies of Mn(II), Cu(II), Zn(II) and Pt(II) dithiocarbamate complexes-crystal structures of the Cu(II) and Pt(II) complexes

Peter A. Ajibade[a]*, Amos A. Fatokun[b]*, Fartisincha P. Andrew[a]

[a]*School of Chemistry and Physics, University of KwaZulu-Natal, Private Bag X01, Scottsville, Pietermaritzburg, 3209 South Africa*

[b]*School of Pharmacy and Biomolecular Sciences, Faculty of Science, Liverpool John Moores University, Liverpool L3 3AF, UK*

ABSTRACT

Mn(II), Cu(II), Zn(II) and Pt(II) complexes of 2-((p-tolylamino)methyl)phenolyldithiocarbamate were synthesized and characterized by elemental analyses and spectroscopic techniques. Spectroscopic studies indicate four coordinate geometry around the metal(II) ions and single crystal X-ray crystallography confirmed the molecular structures of Cu(II) and Pt(II) complexes as distorted square planar. *In vitro* cytotoxic effects of the complexes, indicative of potential anti-cancer properties, were evaluated using human cancer cell lines HeLa and MRC5-SV2, and a normal cell line, MRC5. The complexes exhibited significant toxicity against the cancer cell lines, with IC_{50} values of less than 50µM after 48 h of exposure. Cu(II) and Zn(II) were the most potent and were virtually equipotent in their cytotoxicity against each of the two cancer cells, but only Zn(II) exhibited higher selectivity for a cancer cell than for a normal cell. Mn(II) complex was the least potent, while Pt(II) was the least cancer cell-selective, exhibiting significantly higher toxicity against the parental (normal) MRC-5 cell than against its cancer variant, MRC5-SV2. These compounds could, therefore, inspire the development of inorganic drug leads to generate novel anti-cancer drugs to be delivered directly to the cancerous tissue or through special delivery systems.

Keywords: Dithiocarbamate; Metal(II) complexes; cytotoxicity; anticancer; cancer cells; selectivity.

*Corresponding authors: Peter A. Ajibade (ajibadep@ukzn.ac.za); Amos A. Fatokun (A.A.Fatokun@ljmu.ac.uk)

1. Introduction

The development of metallo-pharmaceuticals has grown rapidly since the discovery of cisplatin and analogues [1, 2]. However, these compounds are associated with side effects such as severe toxicity, intrinsic or acquired resistance and narrow activity range [3, 4]. Some of these side effects are due to reduction in cisplatin uptake and intracellular accumulation [5]. This necessitates the search for alternative metallo-based compounds other than platinum [6-14]. Dithiocarbamate ($R_2NCS_2^-$) ions strongly coordinate and stabilize metal ions in different oxidation states due to the high electron density on the sulphur atoms of the dithiocarbamato moieties [15]. Metal dithiocarbamates have been shown to possess promising biological activities [16, 17]. Recent studies have shown that metal dithiocarbamates bind DNA in different ways, with varying cytotoxic activities [3, 18-25]. They inhibit NF-kB, which is known to promote tumor cell proliferation [26-28]. In continuation of our efforts to develop novel metallo drug candidates [3, 29, 30], we present the synthesis, characterization and *in vitro* anticancer studies of Mn(II), Cu(II), Zn(II) and Pt(II) complexes of 2-((p-tolylamino)methyl)phenolyldithiocarbamate. The molecular structures of the Cu(II) and Pt(II) complexes are presented. Assessment of the anticancer potentials of the complexes focused on their ability both to potently exhibit cytotoxicity and to selectively kill cancer cells, using two cancer cell lines (HeLa, MRC5-SV2) and a normal cell line (MRC5) parental to the MRC5-SV2.

2. Experimental

2.1 Materials and methods

All solvents used in this study were analytical grade and used as obtained without further purification. The infrared spectra of the ligand and metal complexes were recorded on Agilent

Cary 630 FTIR spectrometer (4000-650 cm^{-1}), melting points were recorded on Gallenkamp melting point apparatus and ^{1}H and ^{13}C NMR were recorded on Bruker Avance III 400 MHz, with the carbon and proton shifts presented in ppm in relation to the relevant deuterated solvent signals. The elemental analyses were recorded on Thermoscientific Flash 2000. The UV-Visible spectra were recorded on Agilent Cary 100 UV-Visible spectrophotometer. The molar conductivity and mass spectrometry were recorded on Jenway 4510 conductivity meter and Waters Micromass LCT Premier TOF-MS, respectively. Cell culture media and reagents (DMEM, L-glutamine, antibiotic-antimycotic solution, trypsin solution (TrypLE), phosphate-buffered saline) were obtained from Life Technologies (ThermoFisher Scientific, UK) and Fetal Bovine Serum from Sigma-Aldrich (UK). Chemicals (including doxorubicin) were obtained from Sigma-Aldrich and Tocris Bioscience (Biotechne), UK.

2.2 Synthesis of (2-((p-tolylamino)methyl)phenol)

The secondary amine, (2-((p-tolylamino)methyl)phenol), used for the synthesis of the dithiocarbamate ligand was synthesized according to literature [31]. *P*-toluidine (2.143 g, 0.025 mol) was added to salicylaldehyde (2.7 mL, 0.025 mol) and refluxed at 80°C for 8 h. The solvent was then removed under vacuum to give a yellow oily (Schiff base) product, which was then reduced to secondary amine with sodium borohydride (1.5132 g, 0.04 mol) added in portions at room temperature and stirred for 20 h. The resulting product was extracted with dichloromethane and washed with water to give a solid product after removing the solvent.

Yield, 3.8817 g, 91 %, ^{1}H NMR (400 MHz, $(CD_3)_2CO$, δ, ppm); 8.68(s, 1H), 7.25(d, 1H), 7.05(m, 1H), 6.93(d, 2H), 6.81(m, 2H), 6.66(d, 2H), 5.08(s, 1H), 4.35(d, 2H), 2.18(s, 3H), ^{13}C NMR (400 MHz, $(CD_3)_2CO$, δ, ppm); 45.26(—CH_2—NH—), 20.47(—CH_3), 114.60, 116.12, 129.47, 147.45(—NH—C_6H_4), 156.62, 128.70, 126.42, 120.26, 127.03, 130.24((OH)C_6H_4—),

FTIR (solid, cm^{-1}); 3368 (b), 2903 (m), 2811 (m), 1616 (s), 1582 (s), 1486 (s), 1382 (s), 1222 (s), TOF MS ES+: Calcd $C_{14}H_{15}NO$, m/z: $[M]^+$: 213.12, Found: 214.12

2.3 Synthesis of the dithiocarbamate ligand

The potassium salt of the dithiocarbamate ligand was prepared thus: Aqueous solution of KOH (4 mmol, 0.2244 g) was added to THF solution of the secondary amine (4 mmol, 0.8531 g) and stirred for one hour at room temperature. The mixture was brought down to 0-4 °C and CS_2 (4 mmol, 0.24 mL) was added and stirred for 5 h; diethyl ether was added to form pale yellow precipitate, washed with diethyl ether and dried over silica.

Dithiocarbamate ligand (L): Yield, 1.2446 g, 95 %, m.p 165, Anal. Cal for $C_{15}H_{14}KNOS_2$: C, 55.01; H, 4.31; N, 4.28; S, 19.58. Found: C, 54.76; H, 4.08; N, 4.36; S, 19.33, Λ_m ($\Omega^{-1}cm^2mol^{-1}$); 64.31, ^{1}H NMR (400 MHz, CD_3CN, δ, ppm): 10.13(s, 1H), 7.09(m, 1H), 7.04(q, 2H), 6.77(t, 3H), 6.52(m, 1H), 6.40(q, 1H), 5.65(s, 2H), 2.09(s, 3H), UV-Vis (CH_3CN, λ_{max}), 287 nm (34843 cm^{-1}), TOF MS ES+, m/z $[2M-K]^+$: 615.06, FTIR (ν/cm^{-1}); 1581 (ν_{C-N}), 932 (ν_{C-S}), 3361 (ν_{O-H}).

2.4 Synthesis of the metal(II) complexes C1-C4

The metal(II) complexes **(C1-C4)** were prepared thus: To aqueous solution of the potassium salt of 2-((p-tolylamino)methyl)phenolyldithiocarbamate (0.62 mmol, 0.2031 g), aqueous solutions of the corresponding metals: $MnCl_2 \cdot 4H_2O$ (0.31 mmol, 0.0614 g), $CuCl_2 \cdot 2H_2O$ (0.31 mmol, 0.0528 g), $ZnCl_2$ (0.31 mmol, 0.0409 g), and K_2PtCl_4 (0.31 mmol, 0.1287 g) were added and stirred for 4-12 h. The products were filtered, washed with water and dried over vacuum

to obtain the metal (II) complexes. Crystals suitable for single crystal X-ray crystallography were obtained by slow evaporation of dichloromethane solution of **Cu(II)** complex and slow diffusion of hexane into chloroform solution of **Pt(II)** .

[Mn(L)$_2$], (C1): Yield; 0.1915 g, 98 %, brown solid, Anal. Cal for [$C_{30}H_{28}MnN_2O_2S_4$]: C, 57.04; H, 4.47; N, 4.43; S, 20.30. Found: C, 56.92; H, 4.09; N, 4.64; S, 19.87, m.p; 139 °C, Λ_m ($\Omega^{-1}cm^2mol^{-1}$): 5.46, UV-Vis (CH_3CN, λ_{max}); 270 nm (37037 cm^{-1}), FTIR (ν/cm^{-1}); 1592 (ν_{C-N}), 956 (ν_{C-S}), 3267 (ν_{O-H}).

[Cu(L)$_2$], (C2): Yield; 0.1948 g, 98 %, brown solid, m.p; 172 °C, Λ_m ($\Omega^{-1}cm^2mol^{-1}$): 4.16, Anal. Cal for [$C_{30}H_{28}CuN_2O_2S_4$]: C, 56.27; H, 4.41; N, 4.37; S, 20.03. Found: C, 56.16; H, 4.77; N, 4.89; S, 20.32, UV-Vis (CH_3CN, λ_{max}); 281nm (35587 cm^{-1}), 442 nm (22624 cm^{-1}), TOF MS ES+: Calcd $C_{30}H_{28}CuN_2O_2S_4$, m/z: $[M]^+$: 640.36, Found: 639.03, FTIR (ν/cm^{-1}); 1596 (ν_{C-N}), 951 (ν_{C-S}), 3296 (ν_{O-H}).

[Zn(L)$_2$], (C3): Yield; 0.1716, 85 %, white solid, m.p; 175 °C, Anal. Cal for [$C_{30}H_{28}ZnN_2O_2S_4$]: C, 56.11; H, 4.39; N, 4.36; S, 19.97. Found: C, 56.34; H, 4.17; N, 4.05; S, 20.22, Λ_m ($\Omega^{-1}cm^2mol^{-1}$): 2.66, UV-Vis (CH_3CN, λ_{max}); 281 nm (35587 cm^{-1}), ^{1}H NMR (400 MHz, $(CD_3)_2SO$, δ, ppm); 9.44(s, 1H), 7.30(d, 1H), 7.06(m, 5H), 6.79(m, 1H), 6.71(d, 1H), 5.34(s, 2H), 2.23(s, 3H), ^{13}C NMR (400 MHz, $(CD_3)_2SO$, δ, ppm); 208.06 (C—S), 20.55 (CH_3) 56.82 (CH_2), 114.97, 126.49, 128.59, 154.73 (—$C_6H_4OCH_3$), 118.71, 121.41, 128.31, 129.19, 136.87, 142.70 (—C_6H_4OH), FTIR (ν/cm^{-1}); 1596 (ν_{C-N}), 951 (ν_{C-S}), 3327 (ν_{O-H}). TOF MS ES+: Calcd $C_{30}H_{28}ZnN_2O_2S_4$, m/z: $[M]^+$: 640.03, Found: 639.02

[Pt(L)$_2$], (C4): Yield; 0.2052 g, 86 %, yellow solid, Anal. Cal for [$C_{30}H_{28}PtN_2O_2S_4$]: C, 46.68; H, 3.66; N, 3.63; S, 16.62. Found: C, 46.43; H, 3.39; N, 3.07; S, 16.16, m.p 221°C, Λ_m ($\Omega^{-1}cm^2mol^{-1}$): 4.65, UV-Vis (CH_3CN, λ_{max}); 259 nm (38610 cm^{-1}), 360 nm, (27777 cm^{-1}), ^{1}H NMR (400 MHz, $(CD_3)_2SO$, δ, ppm); 9.66(d, 1H), 7.12(m, 6H), 6.73(m, 2H), 5.09(d, 2H), 2.24(d, 3H), ^{13}C NMR (400 MHz, $(CD_3)_2SO$, δ, ppm); 213.25 (C—S), 21.15 (CH_3) 51.67 (CH_2), 115.62, 127.15, 130.25, 155.89 (—$C_6H_4OCH_3$), 119.38, 120.15, 129.79, 136.84, 138.90, 155.88 (—C_6H_4OH), FTIR (ν/cm^{-1}); 1597 (ν_{C-N}), 948 (ν_{C-S}), 3400 (ν_{O-H}), TOF MS ES+: Calcd $C_{30}H_{28}PtN_2O_2S_4$, m/z: $[M]^+$: 771.90, Found: 772.11

2.5 Single crystal X-ray crystallography

The crystallographic data were obtained on a Bruker SMART APEX2 area detector diffractometer using MoK_a radiation (0.934 Å). The structure was solved with the ShelXS-2013 [32] structure solution program using the Intrinsic Phasing solution method and by using Olex2 [33] as the graphical interface. The model was refined with version 2016/6 of ShelXL [34] using Least Squares minimization.

2.6 In vitro cytotoxicity studies

Three cell lines grown as adherent monolayer cultures were used for the cytotoxicity experiments: Two cancer cell lines (the human cervical adenocarcinoma cell line HeLa and the human foetal lung cancer cell line MRC5-SV2) and one normal cell line (the human foetal lung fibroblast cell line MRC5, which is the parental cell line from which MRC5-SV2 was derived). This approach allows the assessment of the differential sensitivities of cancer and normal cell lines to potential anti-cancer compounds in order to assess the selectivity, or otherwise, of such test compounds for cancer cells. Experiments were conducted largely as previously reported

[4, 35]. The cells were grown in 75cm^2 tissue culture flasks using Dulbecco's Modified Eagle Medium (DMEM) supplemented with 10% Foetal Calf Serum, 2mM L-glutamine and 1% antibiotic-antimycotic solution (containing penicillin, streptomycin and amphotericin B). They were incubated at 37^{o}C in a humidified atmosphere of 5% CO_2. All solutions to which the cultures were exposed were pre-warmed to 37^{o}C. Upon attaining 80-90% confluency in the flask, the cultures were rinsed with phosphate-buffered saline (PBS), trypsinised, harvested into a suspension using the growth medium, counted with a haemocytometer, and seeded into micro-clear, flat-bottom 96-well plates at a density of 7.5 x 10^4 cells per ml (100µL/well, equating to 7500 cells per well). After a period of 24 h, cultures were exposed to a range of concentrations prepared in growth medium (compound stocks were prepared in DMSO but final DMSO concentration that cells were exposed to was not more than 0.1%v/v) as indicated in the results section and added to the cultures, each in triplicate, and plates were incubated for up to 48 h, after which viability was assessed using the MTT (3-(4,5-Dimethyl-2-thiazolyl)-2,5-diphenyl-2H-tetrazolium bromide) assay. This was done by adding to each well 10µL of MTT solution (5mg/mL, prepared in sterile PBS) and incubating the plates for 3 h, after which the content of each well was aspirated and 100µl of DMSO was added to dissolve the insoluble formazan. The absorbance of each well was then read at a wavelength of 570nm using the CLARIOstar plate reader (BMG Labtech). These values are indicative of the viability of the cultures following treatments with the compounds. Changes to the morphology of the cells caused by the treatments were monitored on an Olympus CKX41 microscope fitted with an Olympus DP71 U-TVIX-2 camera. Images were captured using the Olympus cellSens entry software.

For each treatment the mean of the triplicate values was calculated. The mean of the negative control culture was then set to 100% and the mean viability for each concentration normalised

to it. Values are shown as Mean ± SEM (standard error of the mean). Statistical analyses were done using GraphPad (Version 8.0.1) (GraphPad Software, Inc., CA, USA). Statistically significant differences between the means were determined using analysis of variance (ANOVA) followed by a post-hoc test for multiple comparisons (Tukey test). A P-value of less than 0.05 was considered statistically significant. IC_{50} value for each compound was determined using GraphPad by fitting the data to the non-linear regression "log [inhibitor] versus response (3 parameters or 4 parameters (variable slope))". To calculate the Selectivity Index (SI) for each compound, the IC_{50} value for its cytotoxic effect in the normal cell MRC5 was divided by the IC_{50} value for its cytotoxic effect in the cancer variant MRC5-SV2.

3. Results and discussion

3.1 Syntheses

The compounds were prepared as shown in **Scheme 1.** The complexes (**C1-C4**) were obtained as solid in good yield ranging from 67-98%. The molar conductance of the complexes in comparison with that of the ligand in dichloromethane revealed that they were neutral as expected [35]. The elemental analysis and spectroscopic data agree with the proposed four coordinate geometry with two molecules of the dithiocarbamate ligands bonded to the metal(II) ions. Single crystal X-ray crystallography of **Cu(II)** and **Pt(II)** complexes revealed mononuclear four coordinate compounds.

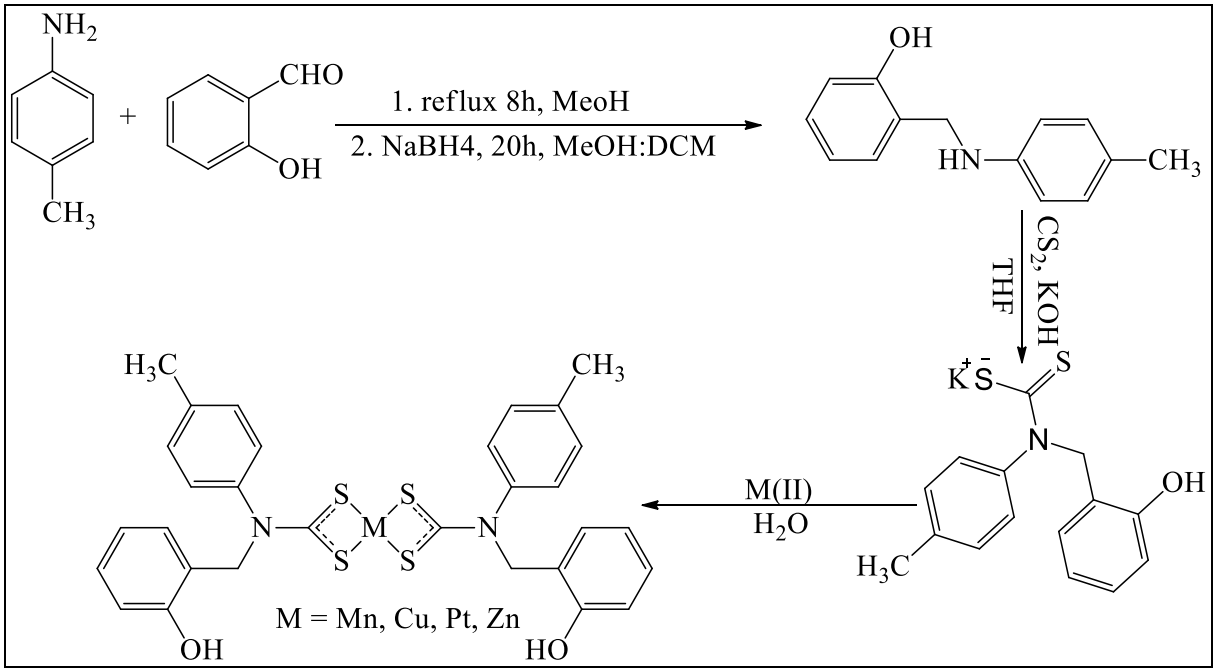

Scheme 1. General synthetic pathway for the preparation of the ligand and the complexes

3.2 Spectroscopic studies

The intense bands observed at 1581 and 932 cm^{-1} in the FTIR spectrum of the free ligand were assigned to the thioureide ν(C—N) and ν(C—S) stretching vibrations of the N—CSS moiety and the broad band observed at 3361 cm^{-1} was assigned to ν(O—H). In the metal complexes, the ν(C—N) stretching vibrations shifted by 14 cm^{-1} to higher energies, which indicates an increase of the carbon—nitrogen double bond character [29, 30, 37]. The ν(C—S) stretching vibrations observed at 932 cm^{-1} in the ligand shifted to 956, 951, 951, and 948 cm^{-1} in the spectra of **Mn(II), Cu(II), Zn(II)** and **Pt(II)** complexes, respectively. This confirms the coordination of the ligand to the metal(II) ions in a bidentate chelating mode via the two sulphur atoms [38-40].

The electronic spectra of the ligand and corresponding metal(II) complexes in dimethyl sulfoxide are presented in **Figure 1**. The band at 287 nm (34843 cm^{-1}) in the electronic

spectrum of the ligand is assigned to the intraligand $n—\pi$ and $\pi—\pi^*$ transitions of the N—CSS moiety of the dithiocarbamate. The Mn(II) (**C1**) is a d^5 complex with zero crystal field stabilization energy in which electronic transitions are both spin and Laporte forbidden, hence no *d-d* transition was observed [41]. The band observed at 270 nm (37037 cm^{-1}) is assigned to ligand to metal charge transfer transitions typical of four coordinate Mn(II) complex [42].

In the electronic spectra of copper(II) complexes in square planar geometry, two absorption bands in the visible region due to $^2B_{1g}\rightarrow{}^2A_{1g}$ and $^2B_{1g}\rightarrow{}^2E_g$ are expected [43, 44]; however, in Cu(II) complex (**C2**)**,** the only band at 442 nm (22624 cm^{-1}) is assigned to $^2B_{1g}\rightarrow{}^2A_{1g}$, while the second band was not observed. In the Zn(II) complex (**C3**), the band at 281 nm (35587 cm^{-1}) is assigned to ligand to metal charge transfer transitions (LMCT) [43]. The electronic spectrum of the Pt(II) complex (**C4**) showed strong and intense absorption at 259 nm (38610 cm^{-1}) and is assigned to intraligand ($\pi—\pi^*$). The *d-d*-transition is masked by charge transfer transition observed at 360 nm (27777 cm^{-1}) [45].

3.3 Molecular structures of the Cu(II) and Pt(II) complexes

The molecular structures of the Cu(II) and Pt(II) complexes are shown in **Figures 2** and **4**. The crystallographic data and structure refinements are presented in **Table 1**. Selected bond lengths and bond angles are listed in **Tables 2** and **3** for Cu(II) and Pt(II), respectively. The Cu(II) complex **C2** crystalized out as centrosymmetric mononuclear entity consisting of two molecules of the dithiocarbamate ligand symmetrically bonded to the Cu(II) ions **(Figure 2).** The geometry around the copper(II) ion in the complex is a four coordinate distorted square planar geometry ascribed to the cis S1—Cu1—S2 of (77.803(19)°) and *trans* S1—Cu1—$S2^1$ of (102.197(19)°) bite angles. The average Cu—S bond length is 2.30 Å in agreement with

reported four coordinate copper(II) dithiocarbamate complexes [29, 46, 47]. The thioureide N—CSS is planar with sp^2 hybridized carbon and the N—CSS bond length of 1.318(3) Å. This is shorter than the C—N single bond (1.465 Å) and longer than C═N double bond (1.279 Å). This indicates partial double bond character of the N—C due to the delocalized π-electron density over the thioureide (NCS_2) moiety [48]. The thioureide S1—C1 and S2—C1 are 1.730(2) Å and 1.723(2) Å, which are shorter than normal C—S single bond length (1.81 Å) but longer than C═S bond length (1.69 Å) [29, 46, 47].

The molecular structure is sustained in the unit cell by non-classical intra molecular C—H···S and secondary inter molecular O—H···S hydrogen bonding (**Figure 3)**. The two aryl rings of the N-substituent are not coplanar with dihedral angle of 67.13° between the two planes (C2, C3, C4, C5, C7, C8 and C10, C11, C12, C13, C14, C15). The non-coplanar nature of these rings may provide some required minimum degree of steric shelter needed for effective drug delivery because of anticipated moderate ligand exchange kinetics.

The Pt(II) complex crystalized out in an orthorhombic crystal system and space group $P2_12_12_1$. The compound is a monomeric (**Figure 4**) four-coordinate platinum(II) center with two molecules of the ligand in a distorted square planar geometry duet to the S1—Pt1—S2 (74.92(12)°) and S3—Pt1—S4 (74.68(12)°) bite angles. The unequal platinum-sulfur bond lengths: Pt1—S1 (2.303(3) Å), Pt1—S2 (2.321(3) Å), Pt1—S3 (2.329(4) Å), Pt1—S4 (2.336(3) Å) indicate the ligands are asymmetrically bonded to the platinum(II) ion [49].
The thioureide C—N bond lengths: N1—C8 (1.290(17) Å) and N2—C16 (1.295 Å) are shorter than normal carbon-nitrogen single bond (1.465 Å) and greater than carbon-nitrogen double bond (1.279 Å) strong carbon-nitrogen double bond character as a result of π-electron density delocalization within the NCS_2 moiety. Also, the thioureide C—S bond lengths are unequal in

the range 1.721-1.755(14) Å and lie between C—S (1.815 Å) and C=S (1.671 Å) bond lengths. This indicates the delocalization of π-electrons in the S—C—S group [50]. The unit cell packing of **[Pt(L)$_2$]** consists of four molecules in a unit cell with non-classical intramolecular C—H···S and O—H···S hydrogen bond interactions.

3.4 Assessment of the potential anticancer properties of the complexes

The cytotoxicity of complexes C1-C4 against cancer cell lines was assessed to determine their potential anti-cancer properties. The three cell lines used, HeLa (cervical cancer cell line), MRC5-SV2 (lung cancer cell line) and MRC5 cells (normal (healthy) lung fibroblast cells), were exposed to the standard drug, cisplatin, and to each of C1-C4, for 24 and/or 48 hours. Cisplatin (6.25-100μM) significantly reduced the viabilities of HeLa, MRC5-SV2 and MRC-5 cells in a concentration-dependent manner, with IC_{50} values, respectively, of 11.1 ± 3.3μM, 8.6 ± 0.3μM and 15.0 ± 0.4μM for 48 h of exposure (Table 4).

The extent of viability reductions caused by cisplatin (or each of the complexes) was consistent with the degree of morphological damage inflicted on the cells (Figure 7). The concentration-dependence of the toxic effects (for cisplatin and the complexes) was also demonstrated morphologically by the progressive worsening of the toxicity phenotype with increasing concentrations. Compared to the negative control cultures that remained adhered to the substratum, appeared confluent and demonstrated network processes consistent with the typical morphology of the different cell types used, the toxicity phenotype was characterized by a rounding up of the cells, shrinkage of the cells and, in some cases, significant loss of cells (Figure 7).

The MRC5-SV2 cell was more sensitive to cisplatin than the HeLa cell, whereas the MRC5 cell was less sensitive to cisplatin than the HeLa cell. On the other hand, both the MRC5-SV2 and the MRC5 cells were more sensitive to the complexes than the HeLa cell. The Selectivity Index (SI) values for cisplatin and the complexes were also determined. SI is the ratio of the IC_{50} value for the toxicity of a compound against a normal cell line (MRC5 in this case) and the IC_{50} value for its toxicity against a cancer cell line or a cancerous variant of the normal cell line (MRC5-SV2 in this case) [51]. A SI greater than 1 suggests the compound is more selective for the cancer cell (desirable), while a SI less than 1 suggests the compound is more toxic to a normal cell than a cancer cell (undesirable). Cisplatin had a Selectivity Index (SI) of 1.7 (48 h) (Table 4), meaning it was nearly twice as toxic to the cancer cell line MRC5-SV2 as it was to its parental (normal) cell line MRC5.

The complexes elicited varying degrees of toxicity. Mn(II) complex **(C1)** was the least toxic (Figure 6D-F), with IC_{50} values (48 h) of 45.6 ± 3.9µM, 37.7 ± 3.0µM, and 29.9 ± 3.9µM, for the HeLa, MRC5-SV2 and MRC5 cells, respectively, translating to a SI of 0.8 (Table 4), which implies it was more toxic to the normal cell line MRC5 than to the cancer variant MRC5-SV2. Both Cu(II) **(C2)** and Zn(II) **(C3)** complexes exhibited concentration-dependent toxic effects, both on viability (Figure 6A-C for Cu(II) and Figure 6D-F for Zn(II)) and on morphology (Figure 7). There was no difference between the toxicities of Cu(II) at 24 h and 48 h.

While Cu(II) and Zn(II) complexes elicited similar toxicity potencies against the two cancer cell lines (HeLa and MRC5-SV2), Cu(II) complex was more toxic to the MRC5 cell line than Zn(II) complex. The IC_{50} values for the effects (48 h) of Cu(II) on HeLa, MRC5-SV2 and MRC5 cells are 30.1 ± 3.5µM, 17.9 ± 2.1µM, and 14.0 ± 3.5µM, respectively, and for Zn(II) the values are 28.1 ± 1.8µM, 19.8 ± 0.2µM, and 22.3 ± 1.9µM (Table 4). Cu(II) produced a SI

of 0.8 while the SI for Zn(II) was 1.1. This means Cu(II) complex exhibited greater toxicity against the normal cell line MRC5 than against its cancer variant MRC5-SV2, whereas Zn(II) complex exhibited marginally greater toxicity against the cancer cell line MRC5-SV2 than against its parental (normal) cell line MRC5.

While Pt(II) complex **(C4)** also reduced the viability of each of the three cell lines in a concentration-dependent manner (Figure 6D-F) and caused morphological damage, it was less toxic to both cancer cell lines (HeLa and MRC5-SV2) than either Cu(II) or Zn(II) complex, but more toxic to the normal cell line MRC5 than either of them (Table 4). This resulted in Pt(II) being the complex with the least SI (0.3), which establishes it as significantly more toxic to the normal cell line (MRC5) than its cancer variant (MRC5-SV2). The ranking orders of potencies for the four complexes are Zn(II)>Cu(II)>Pt(II)>Mn(II) for the HeLa cell line, Cu(II)>Zn(II)>Pt(II)>Mn(II) for the MRC5-SV2 cell line and Pt(II)>Cu(II)>Zn(II)>Mn(II) for the MRC5 cell line. Overall, based on the findings, Zn(II) complex appears the most promising compound that might induce significant death of cancer cells while being selective, at least, mildly, for those cancer cells over normal cells.

However, further studies of the complexes could determine their SIs in a wider selection of cancer cells and their parental (normal) cells in order to ascertain whether the complexes could exhibit differential toxicities and selectivity in different cancer types. Furthermore, as there is now the possibility of using special delivery systems to target anti-cancer drugs specifically to cancer cells and thus spare normal cells [52], all the four complexes could still be investigated for their potential to generate leads for the development of novel, inorganic anti-cancer drugs. They could lend themselves to further modifications to enhance cancer cell toxicity potency and selectivity.

4. Conclusion

Mn(II), Cu(II), Zn(II) and Pt(II) dithiocarbamate complexes were prepared and characterized by elemental analyses, spectroscopic techniques and the Cu(II) and Pt(II) by single crystal X-ray crystallography. Spectroscopic studies confirmed that two molecules of the dithiocarbamate ligand coordinate the metal(II) ions in a bidentate chelating mode to form four coordinate geometry. Single crystal X-ray structures of the Cu(II) **(C2)** and Pt(II) **(C4)** complexes revealed a distorted four coordinate square planar geometry. All the four complexes showed *in vitro* cytotoxic activity against the HeLa and MRC5-SV2 cancer cell lines, with IC_{50} values of less than 50µM. Cu(II) and Zn(II) complexes demonstrated the highest cytotoxicity potencies (IC_{50} values ranging between 20 and 30µM), while Zn(II) was the only ligand that exhibited (marginally) selective toxicity against cancer cells. These complexes, therefore, have potential to generate leads for the development of novel, inorganic anti-cancer compounds.

Acknowledgements

The financial support of Sasol and National Research Foundation (NRF), South Africa is gratefully acknowledged. FP Andrew thanks Tertiary Education Trust Fund (TETfund) and Modibbo Adama University of Technology, Nigeria, for the award of doctoral scholarship. AAF is grateful to the Faculty of Science, Liverpool John Moores University, for the award of a Seed Corn Grant.

Supplementary information

CCDC-1917884 and 1917887 contain the supplementary crystallographic data for this paper. These data can be obtained free of charge at www.ccdc.cam.ac.uk/conts/retrieving.html or

from the Cambridge crystallographic data centre, 12 Union Road, Cambridge, CB2 1EZ, UK; fax: (+44)-1223-336-033 or email: deposit@ccdc.cam.ac.uk]

References

[1] Grafe C, Semrau S, Hein MW, Beckmann A, Mackensen A, Dörje, F. Fromm, M.F., Naunyn-Schmiedeberg's Arch. Pharmacol., 2018, 391, 219-229.

[2] M. Aggarwal, S. Chawla, K. Singh, P. Rana, J. Basic Clin. Pharm., 2018, 9, 118-124.

[3] F. P. Andrew, P. A. Ajibade, J. Mol. Struct., 2018, 1155, 843-855.

[4] R. O. Omondi, D. Jaganyi, S. O. Ojwach, A. A. Fatokun, Inorg. Chim. Acta, 2018, 482, 213-220.

[5] H. Zhu, H. Luo, W. Zhang, Z. Shen, X. Hu, X. Zhu, Drug Des. Dev. Ther., 2016, 10, 1885-1895.

[6] M. R. Williams, B. Bertrand, D. L. Hughes, Z. A. Waller, C. Schmidt, I. Ott, M. O'Connell, M. Searcey, M. Bochmann, Metallomics 2018, 10, 1655-1666.

[7] M. V. Babak, M. Pfaffeneder-Kmen, S. M. Meier-Menches, M. S. Legina, S. Theiner, C. Licona, C. Orvain, M. Hejl, M. Hanif, M. A. Jakupec, Inorg. Chem., 2018, 57, 2851-2864.

[8] D. Havrylyuk, B. S. Howerton, L. Nease, S. Parkin, D. K. Heidary, E. C. Glazer, Eur. J. Med. Chem., 2018, 156, 790-799.

[9] N. Y. S. Lam, D. Truong, H. Burmeister, M. V. Babak, H. U. Holtkamp, S. Movassaghi, D. M. Ayine-Tora, A. Zafar, M. Kubanik, L. Oehninger, T. Sohnel, J. Reynisson, S.M.F. Jamieson, C. Gaiddon, I. Ott, C. G. Hartinger, Inorg. Chem., 2018, 57, 14427-14434.

[10] Q. Du, L. Guo, M. Tian, X. Ge, Y. Yang, X. Jian, Z. Xu, Z. Tian, Z. Liu, Organometallics, 2018, 37, 2880-2889.

[11] L. H. Abdel-Rahman, A. M. Abu-Dief, R. M. El-Khatib, S. M. Abdel-Fatah, Bioorg. Chem., 2016, 69, 140-152.

[12] J. Dam, Z. Ismail, T. Kurebwa, N. Gangat, L. Harmse, H. M. Marques, A. Lemmerer, M. L. Bode, C. B. de Koning, Eur. J. Med. Chem., 2017, 126, 353-368.

[13] L. H. Abdel-Rahman, A. M. Abu-Dief, R. M. El-Khatib, S. M. Abdel-Fatah, J. Photochem. Photobiol., 2016, 162, 298-308.

[14] C. A. Kumar, R. Nagarajaprakash, W. Victoria, V. Veena, N. Sakthivel, B. Manimaran, Inorg. Chem. Commun., 2016, 64, 39-44.

[15] T. Harvey, F. Walsh, A., Nahlé, J. Mol. Liq., 2018, 266, 160-175

[16] Y. J. Tan, Y. S. Tan, C. I. Yeo, J. Chew, E. R. T. Tiekink, J. Inorg. Biochem., 2019, 192, 107-118.

[17] Zia-ur-Rehman, S. Ibrahim, A. Khan, M. Imran, M. M. Naseer, I. Khan, A. Shah, M. N. Tahir, Muneeb-ur-Rahman; I. Z. Awan, J. Coord. Chem., 2016, 69, 551-561.

[18] M. K. Amir, S. Z. Khan, F. Hayat, A. Hassan, I. S. Butler, Inorg. Chim. Acta, 2016, 451, 31-40.

[19] S. S. Al-Jaroudi, M. Altaf, A. A. Seliman, S. Yadav, F. Arjmand, A. Alhoshani, H. M. Korashy, S. Ahmad, A. A. Isab, Inorg. Chim. Acta, 2017, 464, 37-48.

[20] F. Hayat, Zia-ur-Rehman; M. H. Khan, J. Coord. Chem., 2017, 70, 279-295.

[21] Y. S. Tan, K. K. Ooi, K. P. Ang, A. M. Akim, Y.-K. Cheah, S. N. A. Halim, H.-L. Seng, E. R. Tiekink, J. Inorg. Biochem., 2015, 150, 48-62.

[22] S. Shahraki, H. Mansouri-Torshizi, A. Heydari, A. Ghahghaei, A. Divsalar, A. Saboury, H. Ghaemi, M. Doostkami, S. Zareian, Iran. J. Sci. Technol. A, 2015, 39, 187-198.

[23] Y. Li, H. Qi, X. Li, X. Hou, X. Lu, X. Xiao, Apoptosis, 2015, 20, 787-795.

[24] M. K. Amir, F. Hayat, S. Z. Khan, G. Hogarth, T. Kondratyuk, J. M. Pezzuto, M. N. Tahir, RSC Adv. 2016, 6, 110517-110524.

[25] M. Altaf, M. Monim-ul-Mehboob, A.-N. Kawde, G. Corona, R. Larcher, M. Ogasawara, N. Casagrande, M. Celegato, C. Borghese, Z. H. Siddik, Oncotarget 2017, 8, 490-505.

[26] J. Yin, M. Wu, J. Duan, G. Liu, Z. Cui, J. Zheng, S. Chen, W. Ren, J. Deng, X. Tan, Appl Biochem. Biotechnol., 2015, 177, 1716-1728.

[27] M. Xu, K.-N. Wang, K. Wu, X.-P. Wang, Gut Liver, 2015, 9, 411-416.

[28] J. R. Liddell, S. Lehtonen, C. Duncan, V. Keksa-Goldsteine, A.-L. Levonen, G. Goldsteins, T. Malm, A. R. White, J. Koistinaho, K. M. Kanninen, J. Neuroinflammation, 2016, 13, 49-49.

[29] F. P. Andrew, P. A. Ajibade, J. Coord. Chem., 2018, 71, 2776-2786.

[30] F. P. Andrew, P. A. Ajibade, J. Mol. Struct., 2018, 1170, 24-29.

[31] K. K. Manar, M. K. Yadav, M. G. Drew, N. Singh, Polyhedron 2016, 117, 592-599.

[32] G. M. Sheldrick, A short history of shelx. Acta Crystallogr. A, 2008, 64, 112-122.

[33] O. V. Dolomanov, L. J. Bourhis, R. J. Gildea, J. A. Howard, H. Puschmann, J. Appl. Crystallogr., 2009, 42, 339-341.

[34] G. M. Sheldrick, Acta Cryst. C, 2015, 71, 3-8.

[35] R. O. Omondi, S. O. Ojwach, D. Jaganyi, A. A. Fatokun, Inorg. Chem. Commun., 2018, 94, 98-103.

[36] K. M. Oliveira, R. S. Corrêa, M. I. Barbosa, J. Ellena, M. R. Cominetti, A. A. Batista, Polyhedron, 2017, 130, 108-114.

[37] A. A. Isab, M. A. J. Ali, S. Sharif, I. U. Khan, S. K. Kang, T. Khalid, M. Saleem, S. Ahmad, Inorg. Chem. Commun., 2011, 14, 1962-1965.
[38] K. Nakamoto, Infrared and Raman spectra of inorganic and coordination compounds. Wiley: 1977.
[39] K. Nakamoto, Infrared and Raman spectra of inorganic and coordination compounds, applications in coordination, organometallic, and bioinorganic chemistry. Inc, New York 2009.
[40] G. Faraglia, S. Sitran, D. Montagner, Inorg. Chim. Acta, 2005, 358, 971-980.
[41] R. Khajuria, A. Syed, S. Kumar, S. K. Pandey, Bioinorg. Chem. Appl., 2013, 2013, 1-13.
[42] R. Adams, E. Bishop, R. Martin, G. Winter, Aust. J. Chem., 1966, 19, 207-210.
[43] S. M. Mamba, A. K. Mishra, B. B. Mamba, P. B. Njobeh, M. F. Dutton, E. Fosso-Kankeu, Spectrochim. Acta A, 2010, 77, 579-587.
[44] H. Singh, L. Yadav, S. Mishra, J. Inorg. Nucl. Chem., 1981, 43, 1701-1704.
[45] C. E. Housecroft, A. G. Sharpe. Inorganic Chemistry (3rd Edition), Pearson Education Limited 2008.
[46] A. N. Gupta, V. Singh, V. Kumar, A. Rajput, L. Singh, M. G. Drew, N. Singh, Inorg. Chim. Acta, 2013, 408, 145-151.
[47] G. M. De Lima, D. C. Menezes, C. A. Cavalcanti, J. A. Dos Santos, I. P. Ferreira, E. B. Paniago, J. L. Wardell, S. M. Wardell, K. Krambrock, I. C. Mendes, J. Mol. Struct., 2011, 988, 1-8.
[48] A. S. Sonia, R. Bhaskaran, J. Mol. Struct., 1134, 2017, 416-425.
[49] R. S. Amim, M. R. Oliveira, G. J. Perpétuo, J. Janczak, L. D. Miranda, M. M. Rubinger, Polyhedron, 2008, 27, 1891-1897.
[50] A. Z. Halimehjani, K. Marjani, A. Ashouri, V. Amani, Inorg. Chim. Acta, 2011, 373, 282-285.
[51] P. A. Segun, O. O. Ogbole, F. M. D. Ismail, L. Nahar, A. R. Evans, E. O. Ajaiyeoba, S. D. Sarker, Phytother. Res. 2019, 33, 159-166.
[52] J.P. Parker, Z. Ude, C. J. Marmion, Metallomics, 2016, 8, 43-60.

Table 1. Crystal data and structure refinements for Cu(II) and Pt(II)

Compound	$[Cu(L)_2]$	$[Pt(L)_2]$
Formula	$C_{30}H_{28}CuN_2O_2S_4$	$C_{30}H_{28}N_2O_2PtS_4$
$D_{calc.}$/ g cm^{-3}	1.277	1.333
μ/mm^{-1}	0.934	3.888
Formula Weight	640.32	771.87
Size/mm^3	0.33×0.26×0.14	0.37×0.23×0.18
T/K	100(2)	100(2)
Crystal System	triclinic	orthorhombic
Space Group	*P*-1	$P2_12_12_1$
a/Å	7.1091(6)	28.219(6)
b/Å	9.6797(7)	17.750(4)
c/Å	13.6943(10)	7.6800(16)
α/°	69.535(4)	90
β/°	89.651(4)	90
γ/°	71.724(4)	90
V/Å^3	832.65(11)	3846.8(14)
Z	1	4
Z'	0.5	1
Wavelength/Å	0.71073	0.71073
Radiation type	MoK_a	MoK_a
Θ_{min}/°	1.598	2.749
Θ_{max}/°	28.347	25.995
Measured Refl.	15481	13956
Independent Refl.	4126	7216
Reflections Used	3267	6642
R_{int}	0.0313	0.0853
Parameters	183	309
Restraints	0	229
Largest Peak	0.394	3.376
Deepest Hole	-0.316	-1.758
GooF	0.996	1.035
wR_2 (all data)	0.0915	0.1514
wR_2	0.0862	0.1487
R_1 (all data)	0.0510	0.0655
R_1	0.0362	0.0613

Table 2. Some selected bond lengths and bond angles for **[Cu(L)$_2$]**

Atoms	**Angle/°**	**Atoms**	**Length/Å**
S1^1—Cu1—S1	180.0	Cu1—S1^1	2.3076(5)
S2^1—Cu1—S1	102.196(19)	Cu1—S1	2.3076(5)
S2—Cu1—S1^1	102.197(19)	Cu1—S2	2.2948(5)
S2^1—Cu1—S1^1	77.803(19)	Cu1—S2^1	2.2948(5)
S2—Cu1—S1	77.803(19)	S1—C1	1.730(2)
S2—Cu1—S2^1	180.0	S2—C1	1.723(2)
C1—S1—Cu1	83.78(7)	O1—C15	1.369(2)
C1—S2—Cu1	84.33(7)	N1—C1	1.318(3)
S2—C1—S1	113.65(12)	C2—C8	1.381(3)
N1—C1—S1	123.86(16)	C3—C4	1.386(3)
N1—C1—S2	122.46(16)	C4—C5	1.386(4)

Symmetry operation ^{1}-x,1-y,-z; ^{2}1-x,-y,-z; ^{3}+x,-1+y,+z

Table 3. Some selected bond lengths and bond angles for **[Pt(L)$_2$]**

Atoms	**Angle/°**	**Atoms**	**Length/Å**
S1— Pt1— S2	74.92(12)	Pt1—S1	2.303(3)
S1—Pt1—S3	105.05(12)	Pt1—S2	2.321(3)
S1—Pt1—S4	178.45(12)	Pt1—S3	2.329(4)
S2—Pt—S3	179.86(15)	Pt1—S4	2.336(3)
S2—Pt1—S4	105.35(12)	S1—C8	1.755(14)
S3—Pt1—S4	74.68(12)	S2—C8	1.721(14)
C8—S1—Pt1	88.1(5)	S3—C16	1.730(14)
C8—S2—Pt1	88.3(5)	S4—C16	1.726(14)
S2—C8—S1	108.0(7)	C4—C5	1.390(1)
N1—C8—S1	124.1(11)	C4—C7	1.538(15)
N1—C8—S2	127.8(11)	C5—C6	1.390(1)

Table 4: IC_{50} values (mean ± SEM) (in µM) and selectivity indices for the toxicities of the anti-cancer drug, cisplatin, and Complexes C1-C4 against HeLa, MRC5-SV2 and MRC5 cells. Selectivity Index (SI) is the ratio of the IC_{50} value for the toxicity of a compound against a normal cell line (MRC5 in this case) and the IC_{50} value for its toxicity against a cancerous variant of the normal cell line (MRC5-SV2 in this case). A SI greater than 1 suggests the compound is more selective for the cancer cell (desirable), while a SI less than 1 suggests the compound is more toxic to a normal cell than a cancer cell (undesirable).

	IC_{50} (µM)			
	HeLa	**MRC5-SV2**	**MRC5**	**Selectivity Index (SI)**
Cisplatin (standard)	11.1 ± 3.3	8.6 ± 0.3	15.0 ± 0.4	1.7
[Mn(L)2], C1	45.6 ± 3.9	37.7 ± 3.0	29.9 ± 3.9	0.8
[Cu(L)2], C2	30.1 ± 3.5	17.9 ± 2.1	14.0 ± 3.5	0.8
[Zn(L)2], C3	28.1 ± 1.8	19.8 ± 0.2	22.3 ± 1.9	1.1
[Pt(L)2], C4	39.7 ± 10.3	26.9 ± 0.3	7.4 ± 0.9	0.3
Order of potencies (for complexes)	C3>C2>C4>C1	C2>C3>C4>C1	C4>C2>C3>C1	

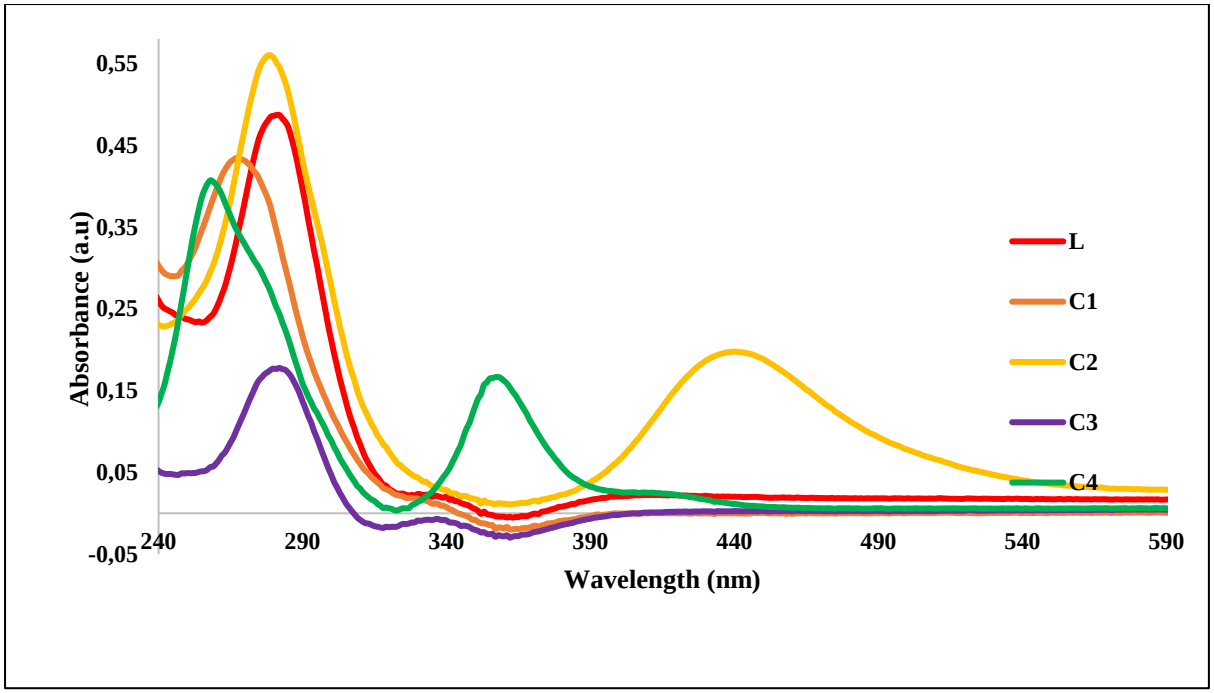

Figure 1. Overlay spectra of the ligand (L) and the complexes: **(C1) Mn(II), (C2) Cu(II), (C3) Zn(II) and (C4) Pt(II)**

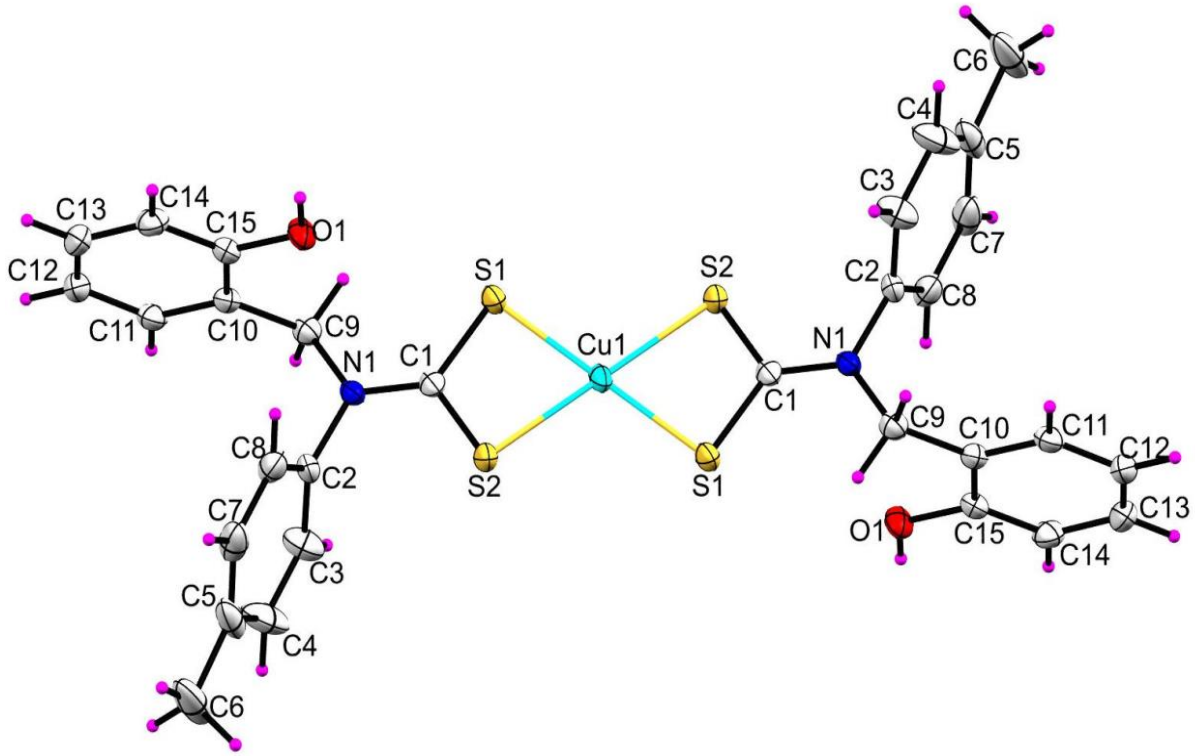

Figure 2. The molecular structure of **Cu(II)** complex with atom numbering thermal ellipsoids 50% probability displacement

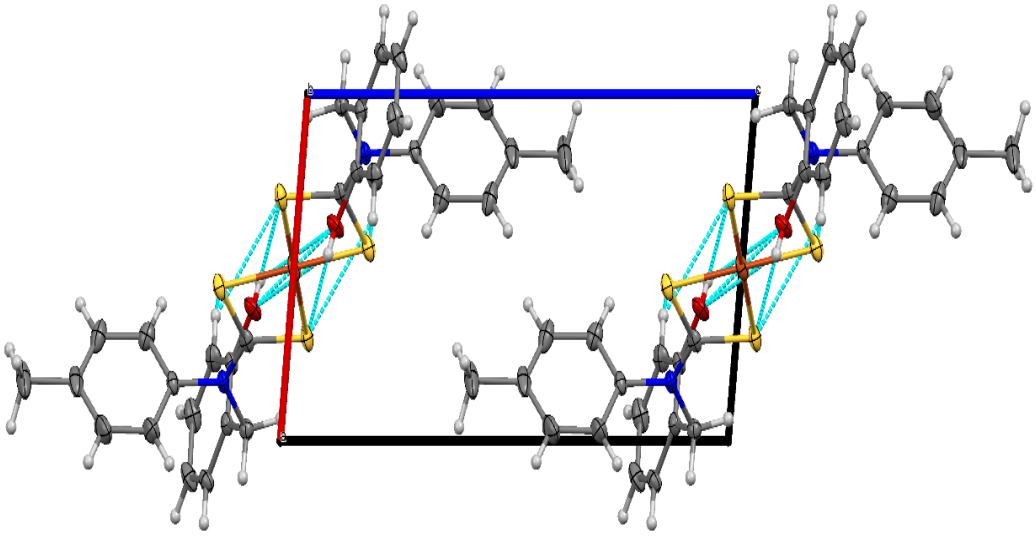

Figure 3. Molecular packing of Cu(II) viewed down crystallographic b-axis of the unit cell with the supramolecular layer sustained by intra molecular C—H···S and O—H···S interactions.

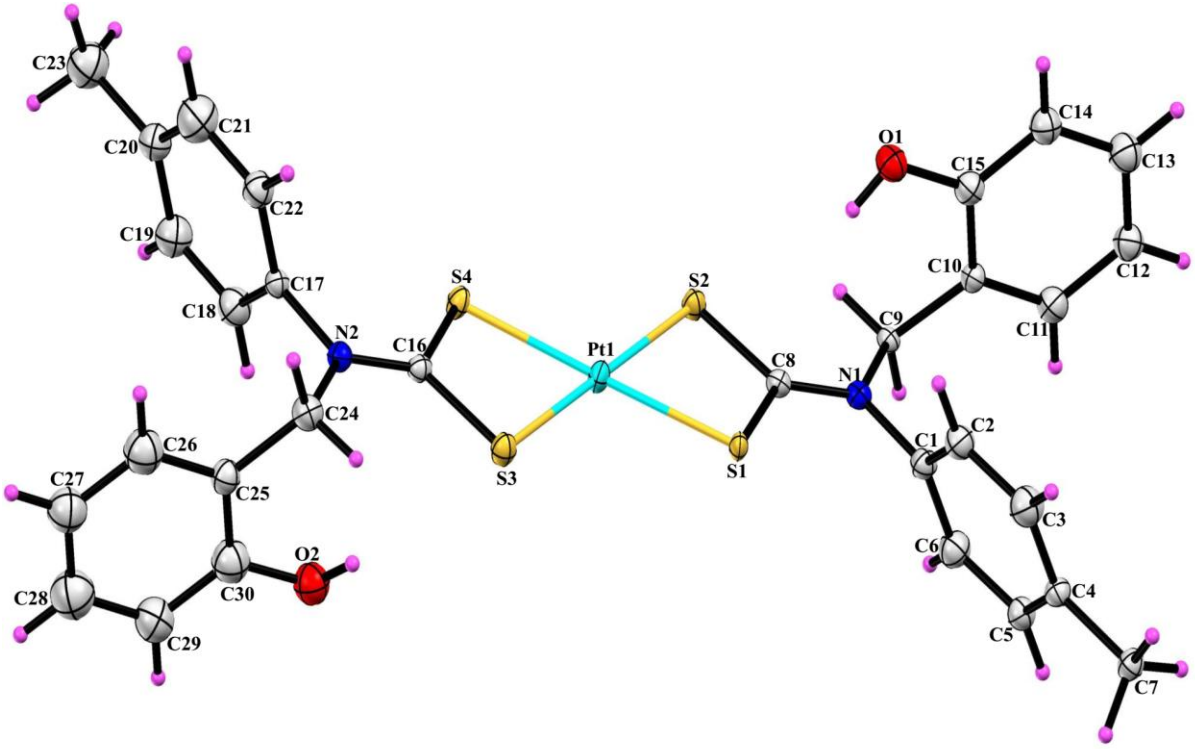

Figure 4. The molecular structure of **[Pt(L)$_2$]** with atom numbering thermal ellipsoids 50% probability displacement

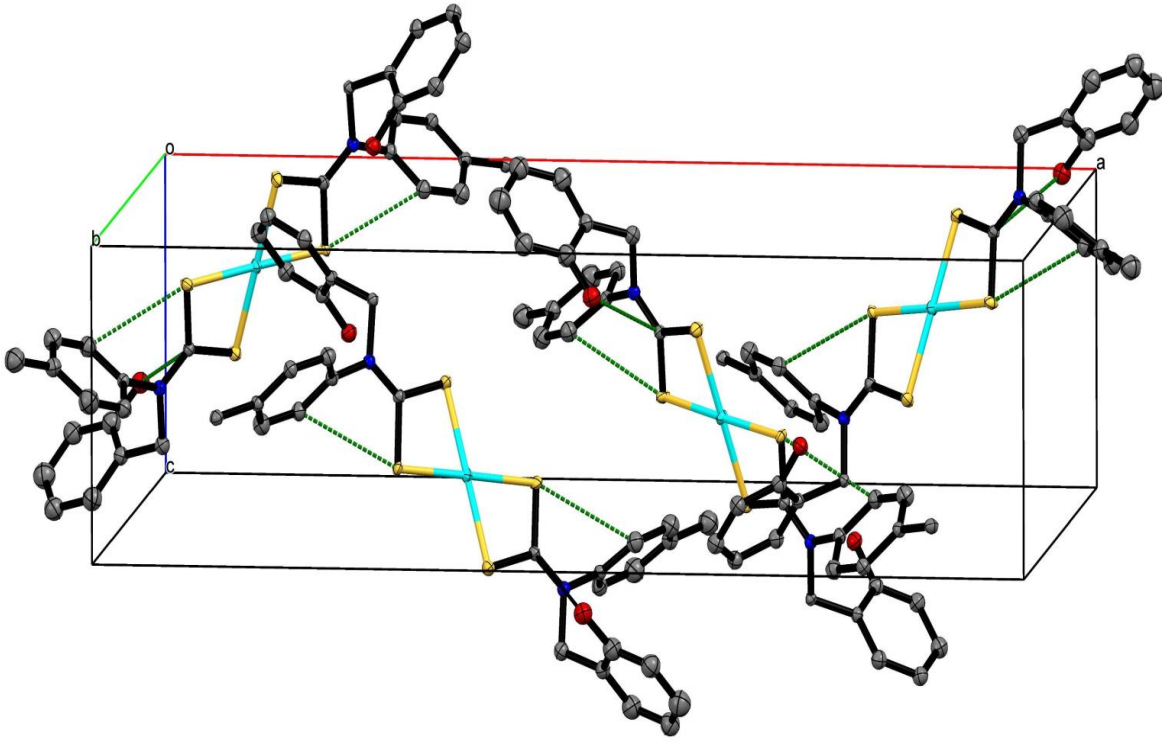

Figure 5. The unit cell packing of **[Pt(L)$_2$]** with hydrogen atoms omitted for clarity and hydrogen bonds in dash green lines

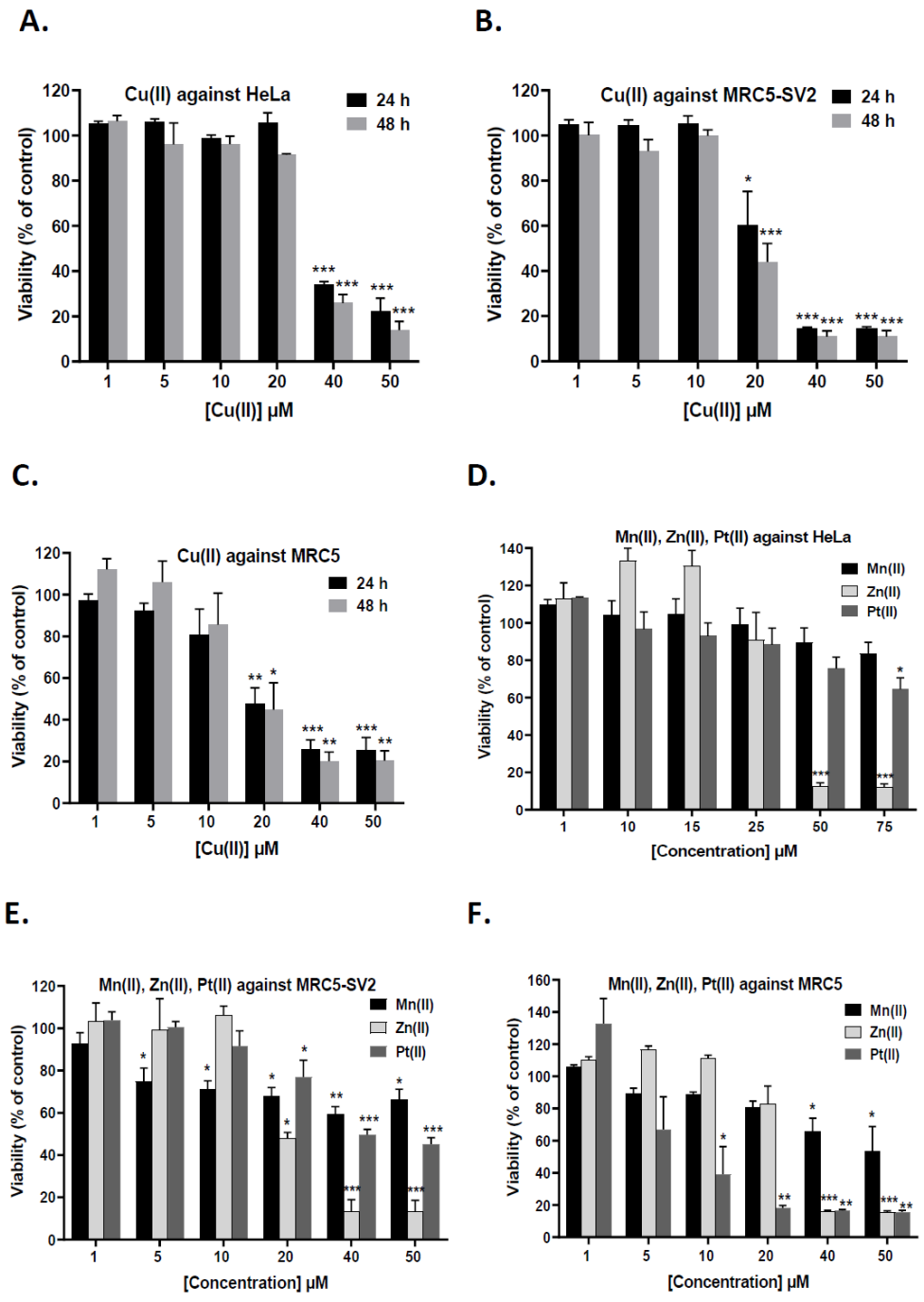

Figure 6: Effects of up to 48 h exposure to Complexes **C1** ([Mn[L]2]), **C2** ([Cu(L)2]), **C3** ([Zn(L)2]) and **C4** ([Pt(L)2]) on the viability of HeLa, MRC5-SV2 and MRC5 cells. (A). Effects of C2 (24 and 48 h) on HeLa cells. (B) Effects of C2 (24 and 48 h) on MRC5-SV2 cells. (C). Effects of C2 (24 and 48 h) on MRC5 cells. (D) Effects of C1, C3 and C4 (48 h) on HeLa cells. (E). Effects of C1, C3 and C4 (48 h) on MRC5-SV2 cells. (F) Effects of C1, C3 and C4 (48 h) on MRC-5 cells. Each bar represents the mean ± SEM of triplicate viability

values obtained as cellular (cytotoxic) response to treatment with the indicated concentration of the indicated compound. *P<0.05, **P<0.001 and ***P<0.0001 compared with negative control. Each data point represents an average of 3 or 4 independent experiments.

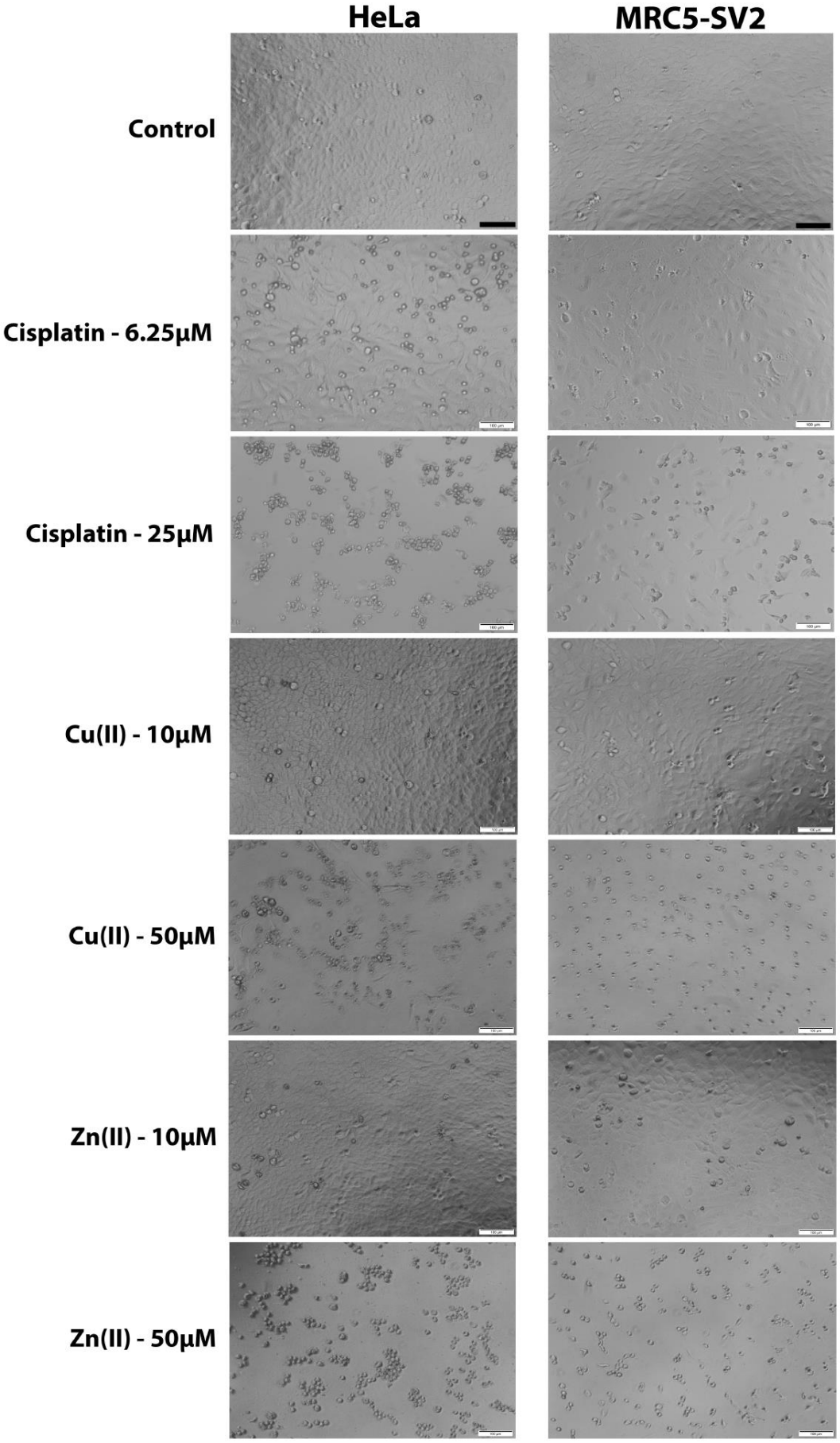
HeLa
MRC5-SV2
Control
Cisplatin - 6.25µM
Cisplatin - 25µM
Cu(II) - 10µM
Cu(II) - 50µM
Zn(II) - 10µM
Zn(II) - 50µM

Figure 7: Representative photomicrographs showing the effects of the anti-cancer drug, cisplatin, and Complexes **C2** ([Cu(L)2]) and **C3** ([Zn(L)2]) on the morphology of HeLa and MRC5-SV2 cells following 48 h exposure to each compound. Bright-field images were acquired with a 10x objective on an Olympus CKX41 microscope fitted with an Olympus DP71 U-TVIX-2 camera. Dead or dying cells are indicated by their rounded and/or shrunken appearance (compared to the control image). Scale bar = 100µm.

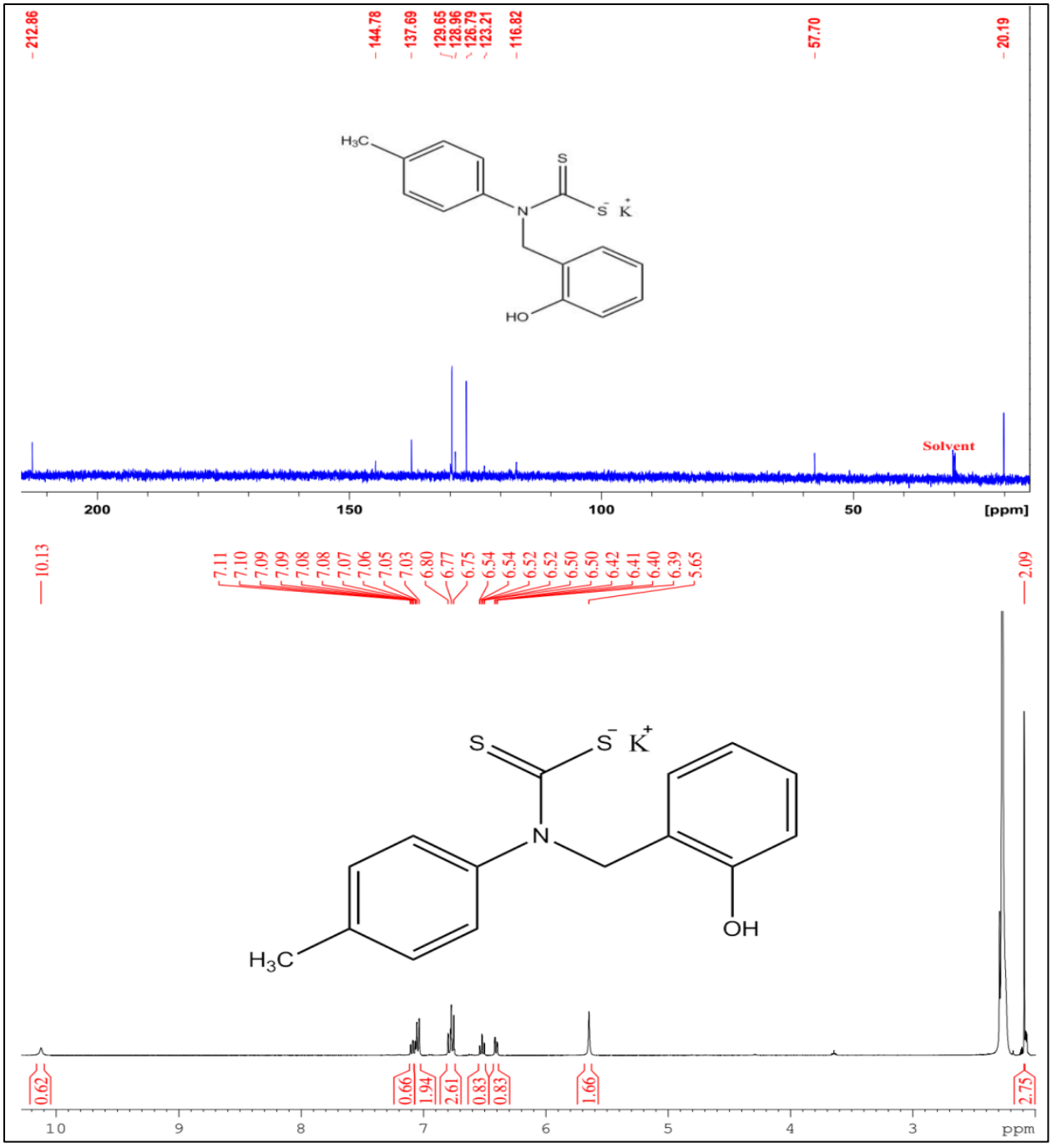

Figure S6. ^{1}H and ^{13}C NMR spectra of ligand (**L**)

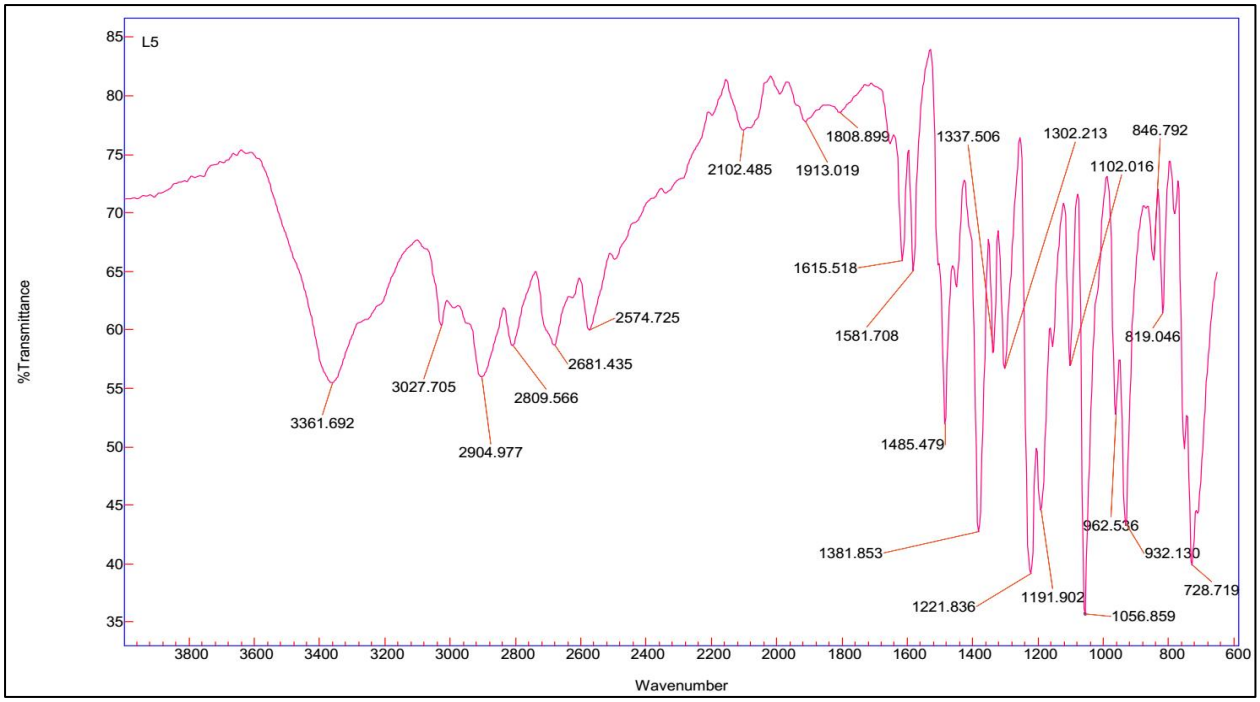

Figure S7. FTIR spectrum of ligand (**L**)

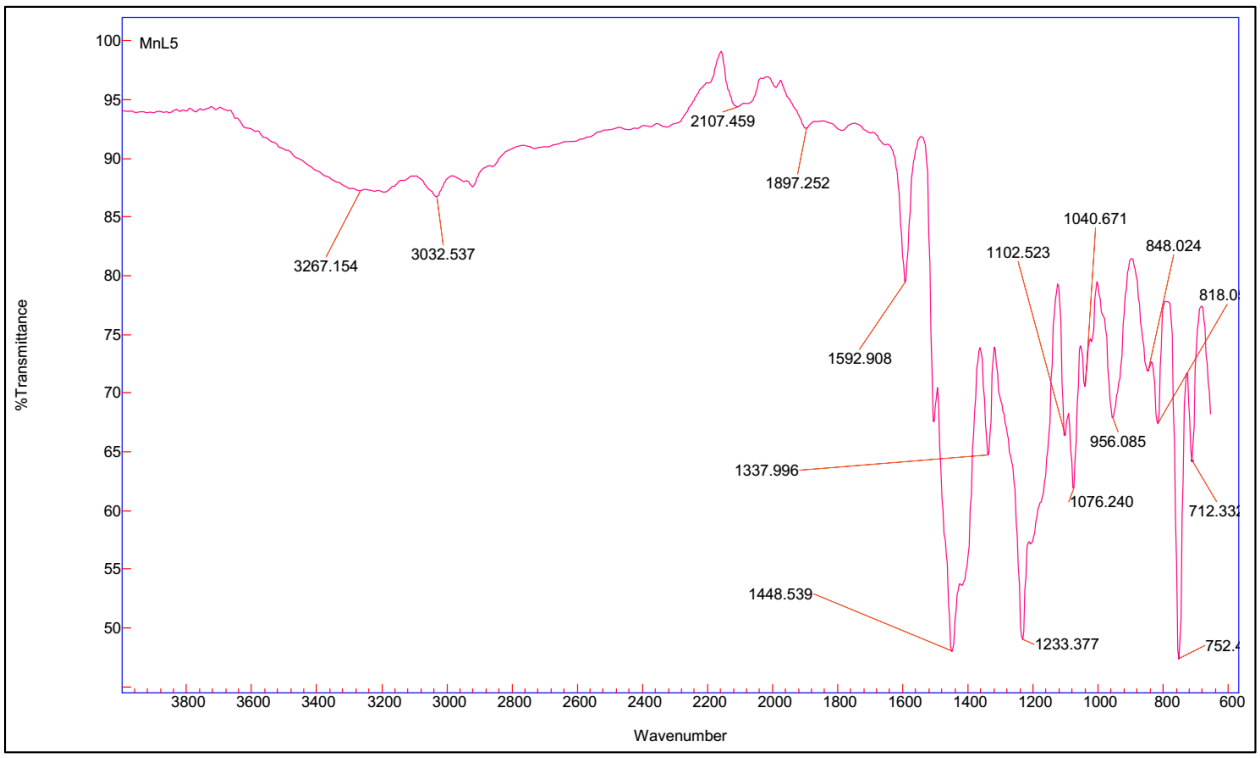

Figure S8. FTIR spectrum of **C1**

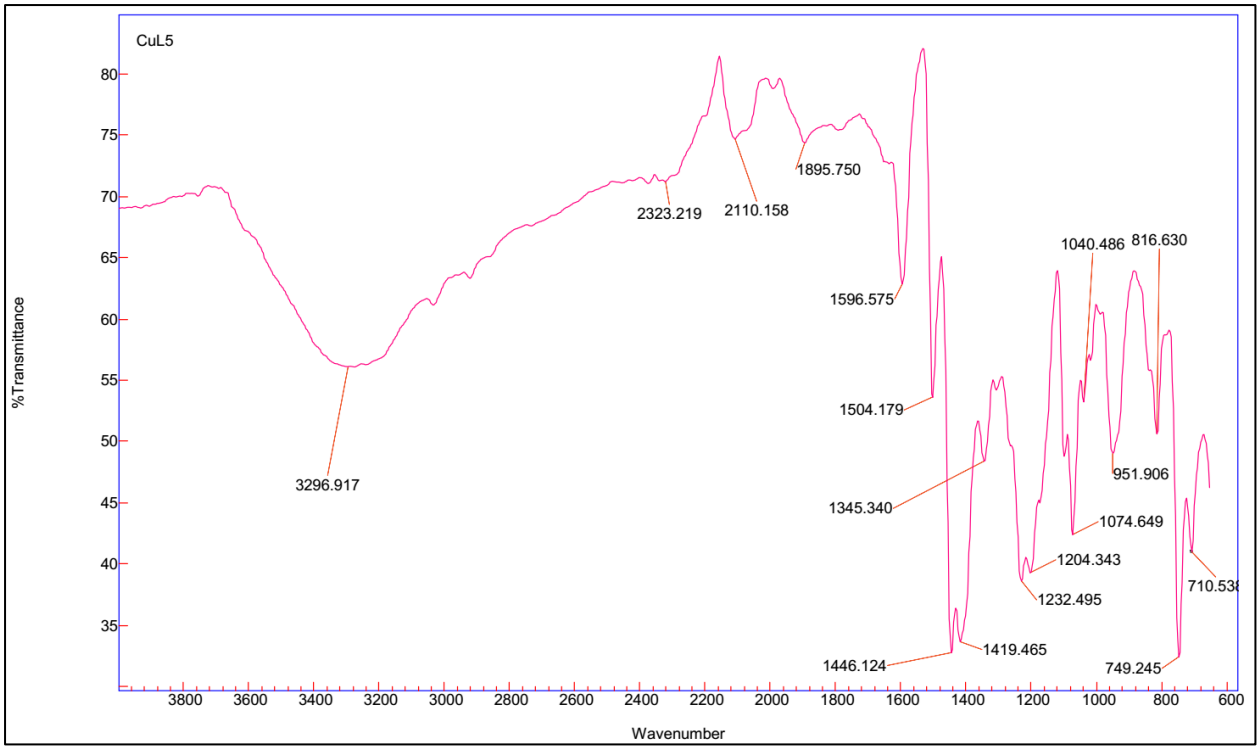

Figure S9. FTIR spectrum of **C2**

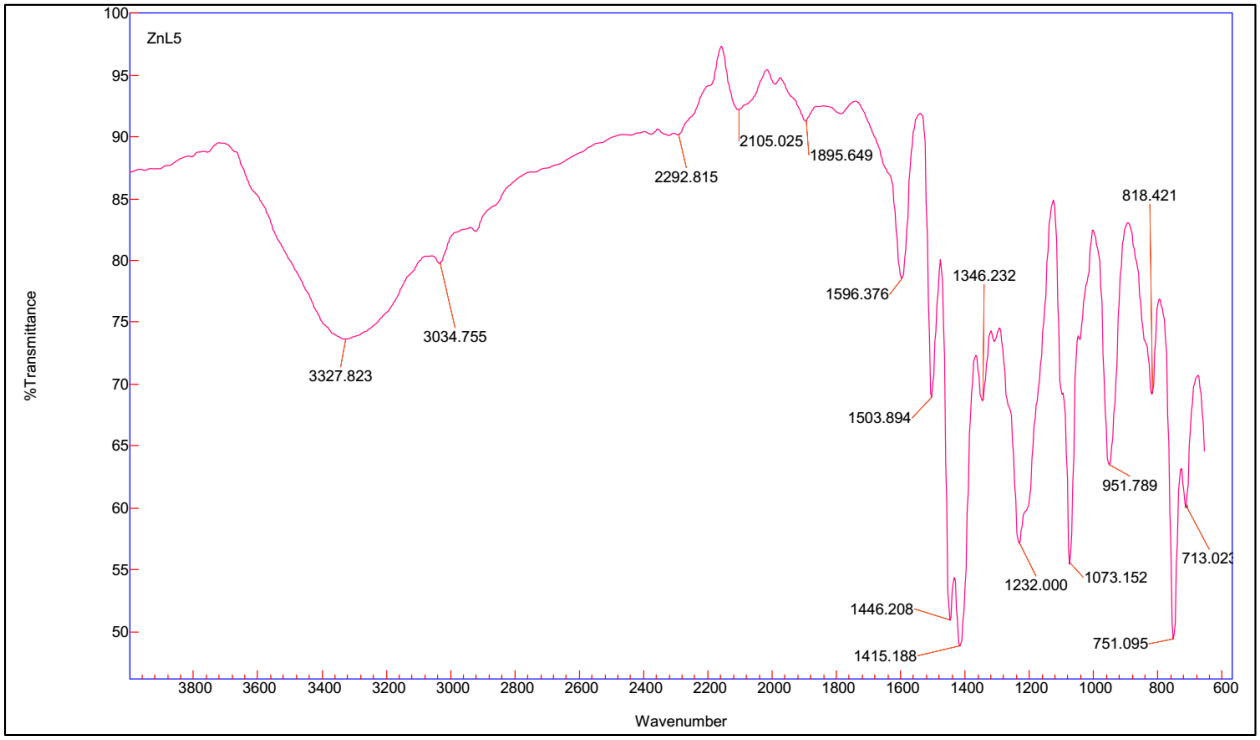

Figure S10. FTIR spectrum of **C3**

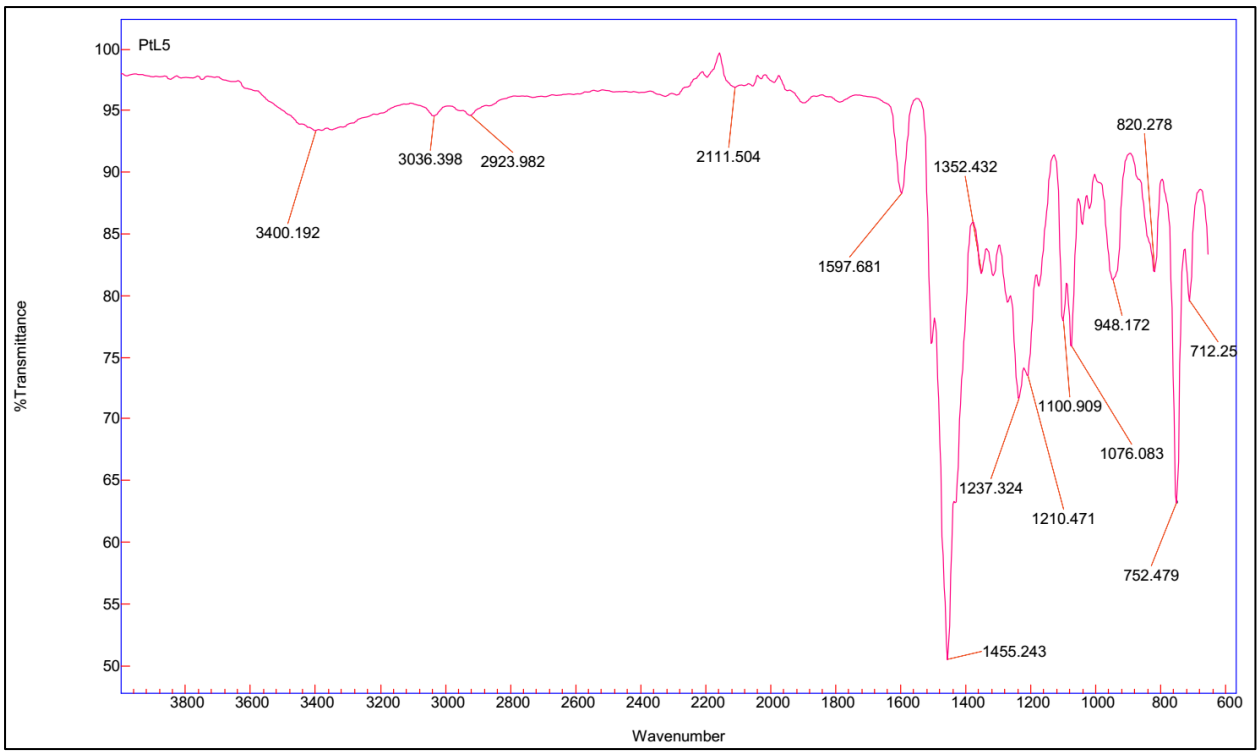

Figure S11. FTIR spectrum of **C4**

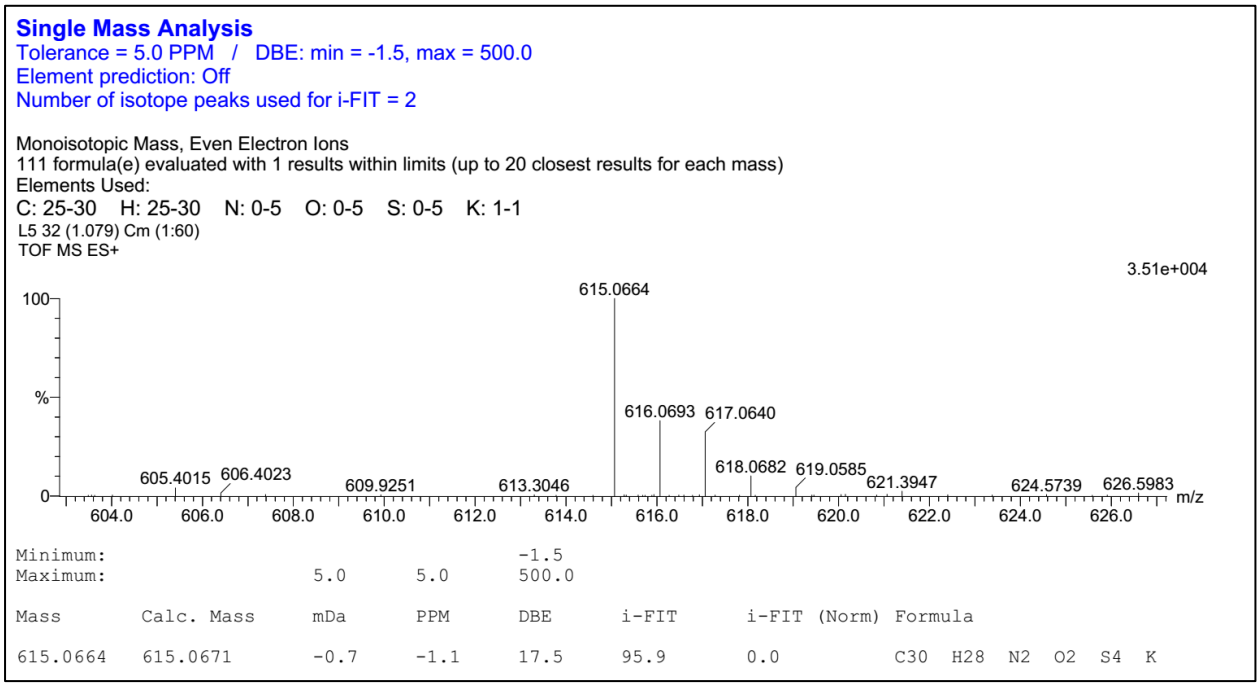

Figure S12. Mass spectrum of ligand **(L)**

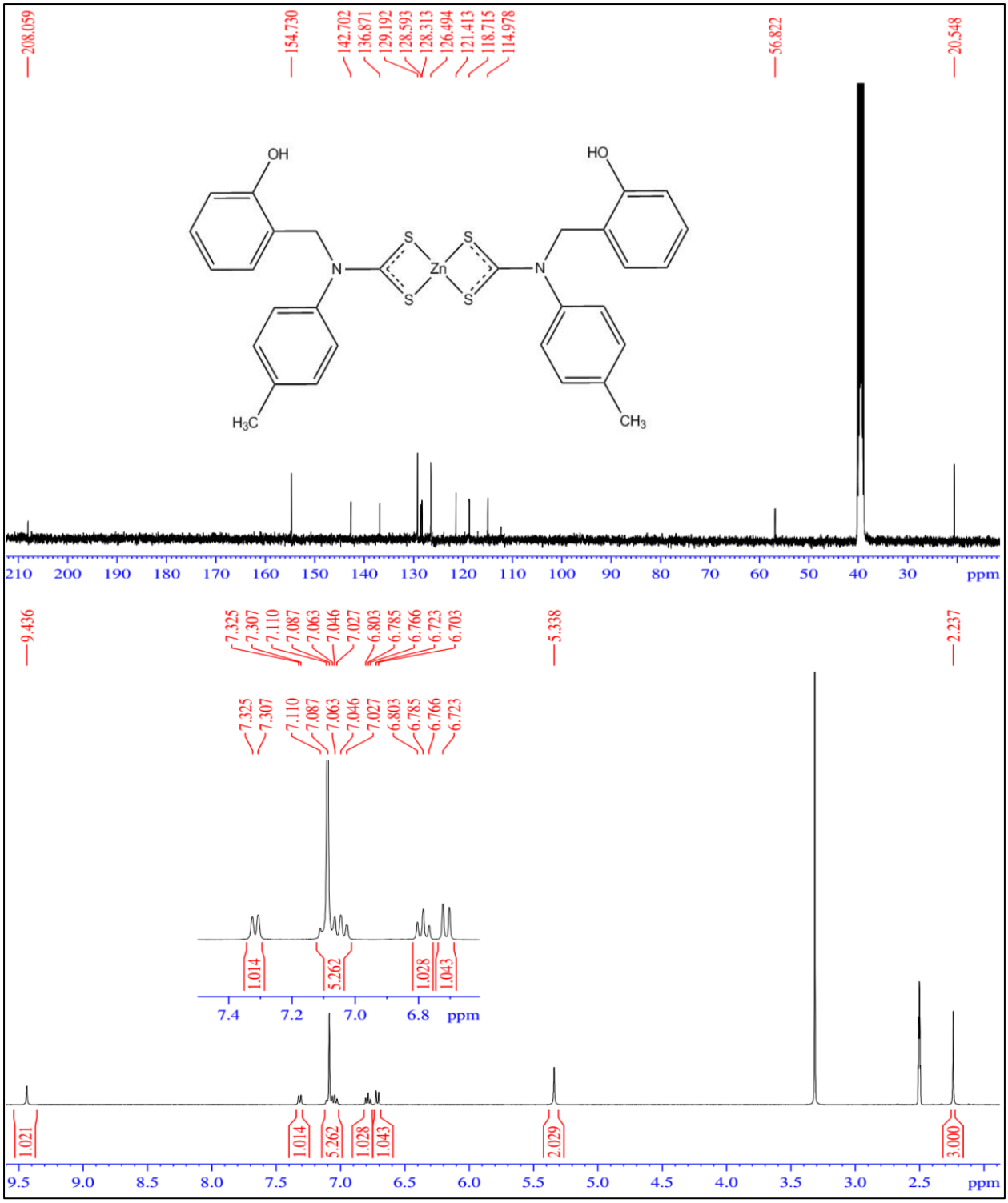

Figure S13. ^{1}H and ^{13}C NMR spectra of **C3**

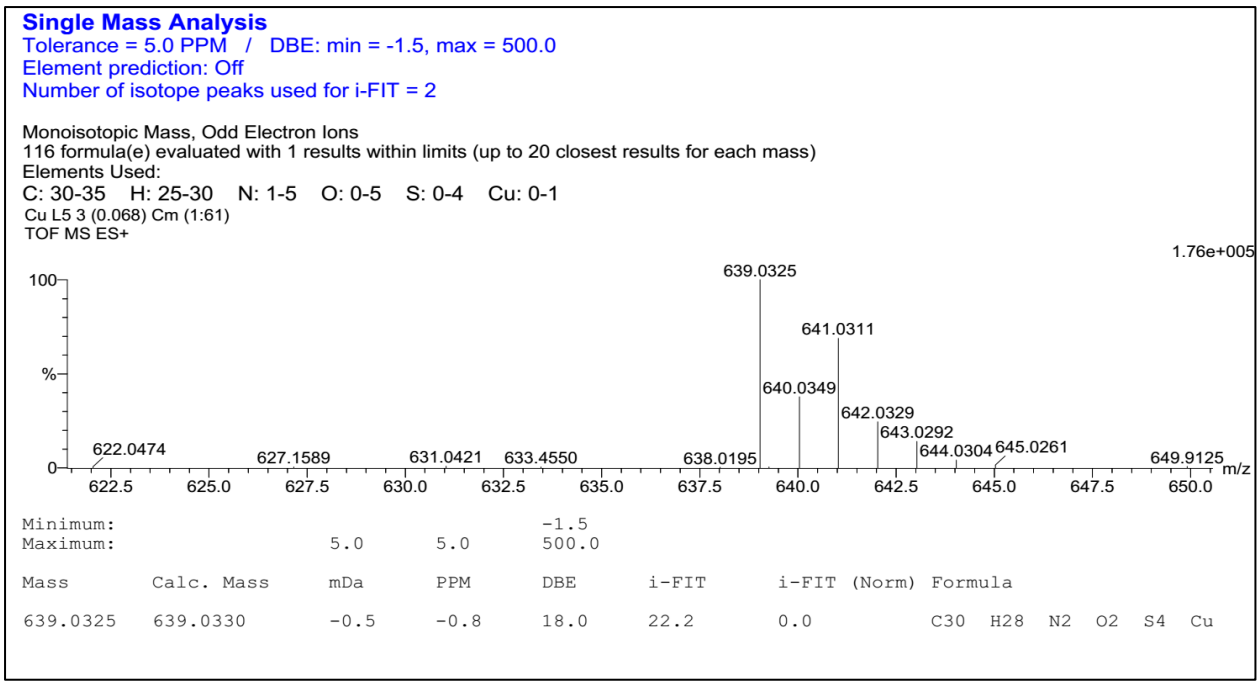

Figure S14. Mass spectrum of C2

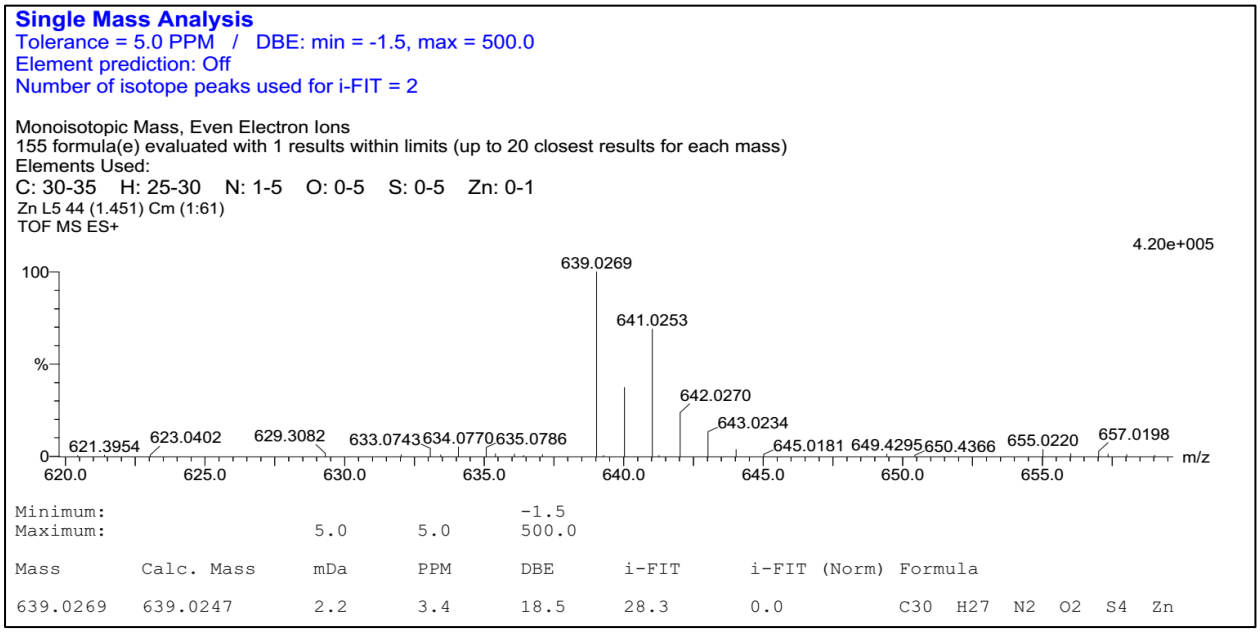

Figure S15. Mass spectrum of C3

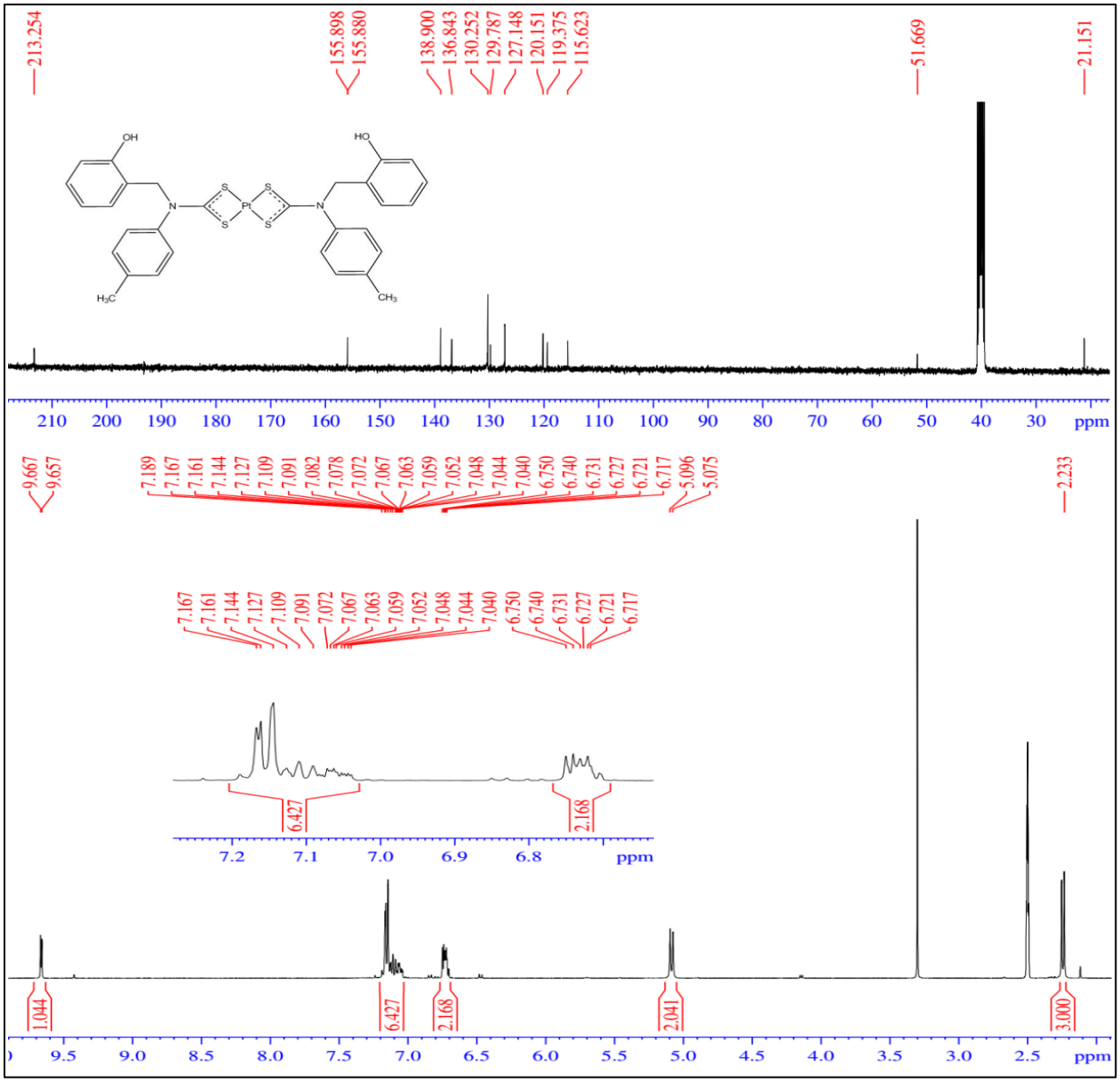

Figure S16. ^{1}H and ^{13}C NMR spectra of **C4**